Int J Fatigue **13** No 4 (1991) pp 303–312

Compression fatigue behaviour of notched carbon fibre–epoxy laminates

C. Soutis, N.A. Fleck and P.A. Smith

The compression fatigue behaviour has been studied for $[(\pm 45/0_2)_3]_s$ carbon fibre–epoxy specimens containing either a single hole or two closely spaced holes. For both single-hole and two-hole specimens, fatigue damage consists of ply cracking, delamination and, at loads approaching the static compressive strength, fibre microbuckling. When the applied maximum compressive stress is below 85% of the static compressive strength (denoted throughout the paper as σ_{ult}) no fatigue failures occur prior to reaching 10^6 cycles. After fatigue cycling at peak loads smaller than 85% of σ_{ult} the residual strength of the specimen was found to increase as a result of longitudinal splitting and associated damage which acts to reduce the stress concentration at the hole edge. This effect has been modelled for the single-hole specimen using a two-dimensional finite element analysis. At peak fatigue loads equal to 90% of σ_{ult} fatigue failure occurs as a result of microbuckle initiation and growth. The presence of zinc iodide solution (which is used as a penetrant in X-ray studies) has been shown to accelerate split growth and thereby prolong the fatigue life of the specimens.

Key words: compression fatigue; carbon fibre–epoxy laminates; microbuckling

The behaviour of composite laminates under compressive loading is less well understood than their behaviour under tensile loading and is currently one of the limiting design features. In earlier work by Soutis[1] and Soutis and Fleck,[2] the static compressive behaviour was characterized for $[(\pm 45/0_2)_3]_s$ T800/924C carbon–epoxy laminates containing either one or two holes. Of particular interest in these works was the initiation and growth of microbuckled regions in the 0° plies at the hole edges. This mechanism has been observed by other workers testing various lay-ups (*eg* Purslow and Potter,[3] Guynn and Bradley[4]) and the growth of these microbuckles under static loading has recently been modelled analytically by Soutis *et al.*[5] The behaviour of notched laminates under compressive fatigue loading is of considerable practical interest for recently developed carbon fibre reinforced plastic (CFRP) systems, where there are indications that compression fatigue may be of concern, cf. Curtis.[6]

In the present paper we describe the compression fatigue behaviour of a CFRP laminate with a single hole. Tests were also performed on specimens containing two adjacent holes, and the interaction of fatigue damage between the two holes was examined. We used a $[(\pm 45/0_2)_3]_s$ balanced lay-up made from Toray 800 fibres in a Ciba-Geigy 924C epoxy resin. Toray 800 fibre is an exceptionally high strength carbon fibre and is used in aerospace applications. The aims of the study were to determine the stress–life behaviour, to study the various damage mechanisms which occur in compression fatigue, and to assess their effect on residual strength.

Experimental procedure

Material and specimen configuration

The test specimens were 245 mm long by 50 mm wide, cut from T800/924C CFRP $[(\pm 45/0_2)_3]_s$ panels, giving a gauge length of 116 mm after tabbing. Two different configurations were used for fatigue testing: single hole and two holes. The two holes were drilled symmetrically about the longitudinal axis of the specimen, with their centres on the transverse symmetry axis. The holes were placed one radius apart from hole edge-to-edge. The diameter of the holes was 5 mm.

In all the fatigue tests an anti-buckling device was employed to prevent gross column buckling, Soutis *et al.*[2,5] Its window size was 90 mm long by 38 mm wide, allowing local microbuckling associated with delamination around the hole(s) to occur, but restraining the specimen from general buckling. Teflon tape was used on the inside surfaces of the fixture to reduce friction. Concern was given throughout the testing procedure to the alignment of the specimen in the lower and upper grips and to the proper attachment of the anti-buckling guides to the specimen. Misalignment of the load axis causes out-of-plane deflection, unsymmetric damage development through the laminate thickness and premature specimen failure.

Test details

Compression–compression fatigue tests were run on a servo-hydraulic testing machine under load-controlled constant-

0142-1123/91/040303–10

amplitude, sinusoidal axial loading at a frequency of 10 Hz. At this frequency hysteretic heating effects are believed to be negligible for the material system studied. Maximum load levels were equal to 75, 85 and 90% of the static notched compressive strength (σ_{ult}), and a load ratio R (= minimum load/maximum load) of 10 was used.

Damage monitoring techniques

The damage that occurred during fatigue loading was monitored by using penetrant-enhanced X-ray radiography. Care has to be taken using this technique because the presence of penetrant may affect the subsequent damage growth.

Some of the damaged specimens were sectioned with a diamond circular saw and sections were then polished for examination by light microscopy. These section studies are useful for identifying the particular ply interface at which delamination occurs and for locating matrix cracking. This technique was also used to observe fibre microbuckling in detail, which is not possible with X-ray radiography: a zone of fibre microbuckling on an X-ray radiograph resembles a crack.

The effect of compressive fatigue damage on the stiffness of the single-hole specimens was measured throughout the fatigue test by recording the elongation of the specimen using a displacement clip gauge. The clip gauge had a gauge length of 70 mm and was fastened to knife edge anvils glued to the specimen. The anvils were placed along the longitudinal centre line of the specimen, and were symmetrically disposed with respect to the hole. The clip gauge was used periodically during the fatigue test to measure displacement range over a fatigue cycle. To achieve this, the test frequency was reduced from 10 Hz to 0.01 Hz and displacement readings were taken manually.

Experimental results and analysis, single-hole specimens

Damage development during compression fatigue

$\sigma_{max} = 75\%\ \sigma_{ult}$

Figure 1 shows a typical sequence of X-ray radiographs detailing the damage development in compression–compression fatigue at σ_{max} = 75% σ_{ult} = 320 MPa (stress values are based on the cross-sectional area). The dark circular band around the hole present in the initial radiograph is a combination of drilling damage and zinc iodide residue on the hole interior. Within the first 100 cycles 0° ply cracks appear at the top and bottom of the hole, see Fig. 1(a). Longitudinal splits occur tangential to the hole in the 0° layers after about 10^3 cycles. These splits extend in length with increasing number of cycles and serve as the outer boundaries to the damage occurring above and below the hole, as shown in Fig. 1(b). Many small matrix cracks in the ±45° layers exist along these splits. The growth rate of the splits tangential to the hole was estimated from the series of radiographs and was found to decrease with increasing split length, see Fig. 2.

After approximately 10^5 cycles, delamination develops at the ±45°/0° ply interfaces. Delamination initiates in areas which have seen extensive matrix cracking. This becomes quite evident at 10^6 cyles, as shown in Fig. 1(c). At 10^6 cycles, in the region between the 0° splits above and below the hole, axial and off-axis cracks develop, allowing

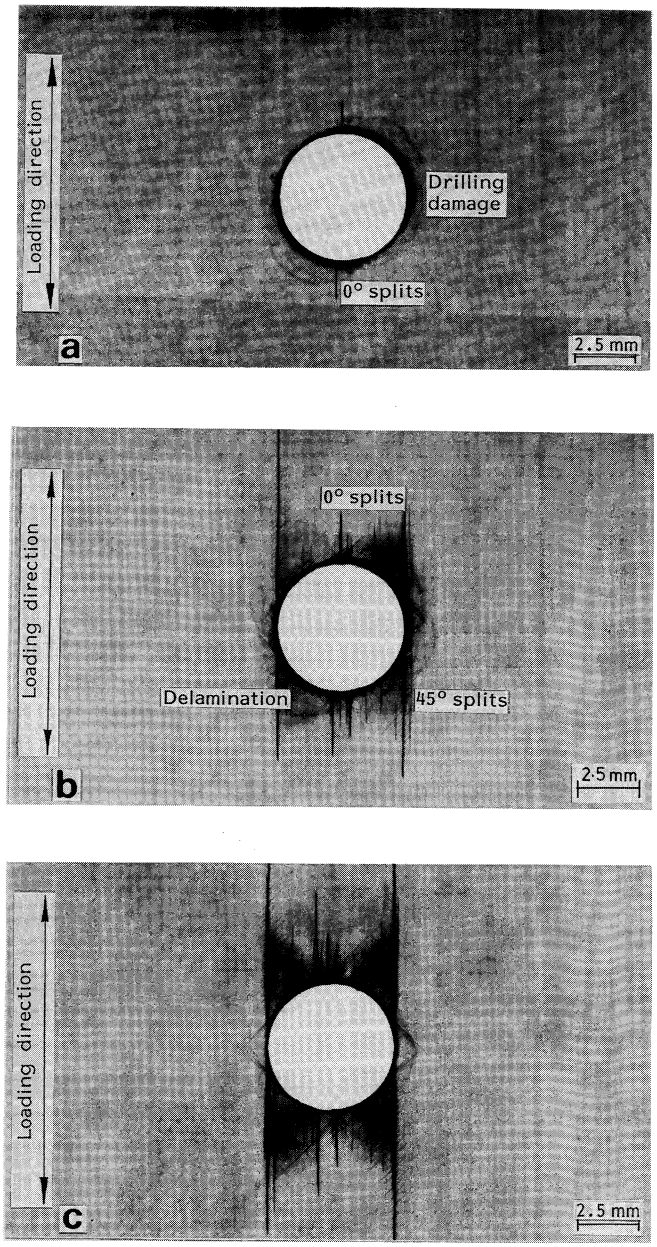

Fig. 1 X-ray radiograph showing compression–compression fatigue damage in a specimen with a 5 mm diameter hole, cycled at σ_{max} = 75% σ_{ult} (=320 MPa) (a) after N = 100 cycles. (b) Fatigue damage after N = 10^5 cycles. (c) Compression–compression fatigue damage after 10^6 cycles (stress level = 75% σ_{ult})

delamination to grow longitudinally. Delamination extends above and below the hole but is arrested in lateral growth by the presence of the 0° tangential cracks. At this applied stress level no fatigue failure was observed prior to reaching 6 × 10^6 cycles, at which point the test was terminated.

The X-ray radiograph in Fig. 3 illustrates the damage of a notched specimen fatigued without test interruption for 10^6 cycles at σ_{max} = 75% σ_{ult}. Zinc iodide solution was applied to this specimen only at the end of the test. It can be seen that the damage is not as extensive and that the matrix splits are about 40% shorter than those observed in Fig. 1, where the test was interrupted at regular intervals and zinc iodide solution was applied. This suggests that the penetrant increases the extent of the damage. Theoretical models of composite failure are often based upon damage growth data, where zinc iodide solution is used to monitor the damage. These studies

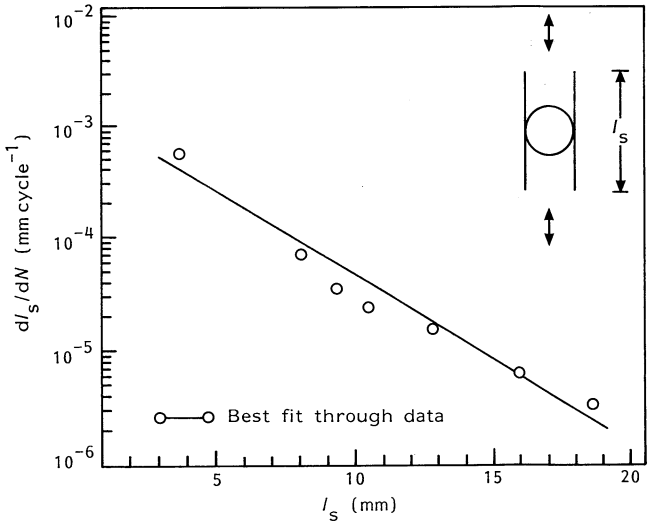

Fig. 2 Split growth rate versus split length for a single-hole specimen cycled at stress level = 75% σ_{ult}

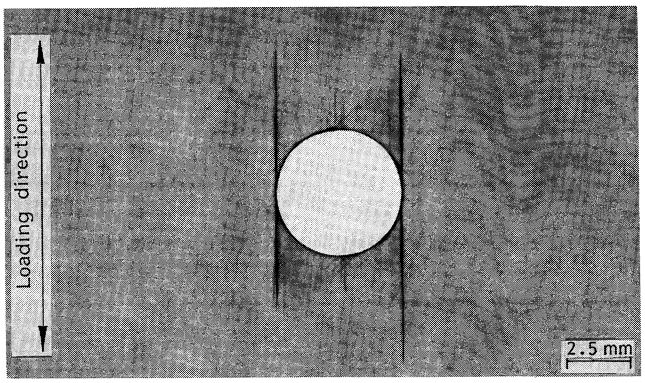

Fig. 3 X-ray radiograph illustrating compression–compression fatigue damage on a specimen cycled continuously up to 10^6 cycles at a stress level of 75% σ_{ult} (=320 MPa)

implicitly assume that the penetrant (in this case zinc iodide solution) has no effect on the damage growth rate. The models require re-calibration if they are to predict the life of a service component where zinc iodide solution is not applied.

Transverse sectioning and microscopic examination enable individual matrix cracks in the 0° layers to be observed. A matrix crack in a single 0° ply constrained on both sides by ±45° plies does not grow directly into the neighbouring layers since this would require fracture of the ±45° fibres. The interfaces between plies of dissimilar orientations either arrest the crack or delaminate. Figure 4 shows a micrograph of a typical cross-section of a specimen cycled at σ_{max} = 75% σ_{ult} for 10^6 cycles. The matrix cracks within the 0° layers and associated delaminations are evident.

The fatigue damage described above tends to reduce the notched specimen effectively into two unnotched laminates on each side of the hole, separated by damaged material. Consider the notched specimen which was fatigued without interruption for 10^6 cycles. The residual compressive strength of the specimen is 506 MPa, which corresponds to a 15% increase in strength. Other workers have made similar observations. Whitcomb,[7] for example, inferred from his experimental work (tensile and compressive fatigue behaviour of carbon–epoxy laminates) that matrix splitting can reduce the notch stress concentration significantly, leading to an increase in the residual strength of the damaged laminate. He measured residual strengths which were greater than or equal to the original strength of the composite laminate. In the present work, two-dimensional finite element calculations have been performed in an attempt to account for the increase in residual strength due to splitting and to delamination. The method and results are presented in the next section.

Compression fatigue loading at the stress σ_{max} = 75% σ_{ult} (=320 MPa) causes a decrease in stiffness of approximately 5% over the whole life, across the gauge length used in the current work. This is consistent with the observation that the damage is restricted to the vicinity of the hole, see Fig. 1(c). Similar measurements were made by Black and Stinchcomb.[8] They investigated the damage development mechanisms in $[\pm 45/0_2/\pm 45/0_2/\pm 45/0/90]_{2s}$ notched graphite/epoxy laminates during constant-amplitude compressive fatigue loading and found that the longitudinal stiffness does not decrease significantly during cyclic loading.

σ_{max} = 85% σ_{ult}

Damage development at the stress level of σ_{max} = 85% σ_{ult} (=365 MPa) is qualitatively similar to that observed at 75% σ_{ult} but is more severe in extent. Figure 5 shows damage after 10^6 cycles. The residual compressive strength of this specimen is 520 MPa after 10^6 cycles, which corresponds to a 20% increase in strength over the undamaged specimens with 5 mm diameter holes. As with the specimens tested at 75% σ_{ult} this increase is attributed to the redistribution of stress around the hole due to the relieving of the stress concentration in the 0° plies by the splitting and delamination.

σ_{max} = 90% σ_{ult}

At a maximum cyclic compressive stress of σ_{max} = 90% σ_{ult} (=387 MPa) a specimen failed in fatigue after 6×10^4 cycles. Fibre microbuckling develops on the first loading cycle; it occurs in the 0° layers at the edges of the hole, which is the location of the highest in-plane compressive stresses. A microbuckle zone propagates from each edge of the hole by fatigue across the specimen width. The microbuckles are inclined at an angle of 10° to the horizontal axis, and catastrophic failure occurs when they reach a length of 3 mm. It appears that the stress relieving effects associated with splitting and delamination are not sufficient to arrest the microbuckle growth. The post-failure appearance of the specimen was similar to those tested under static loading. At this high stress level only one fatigue test was conducted. The test set-up was insufficient to generate the high compressive loads needed to fatigue the specimen at 90% σ_{ult}. Thus, no microbuckling growth data were obtained from the single-hole specimen at this load level.

Finite element analysis

Under fatigue loading, splits develop in the 0° layers tangential to the hole, as shown in Figs 1(b) and 1(c). An elastic two-dimensional finite element analysis, implemented in the MARC package,[9] was performed on a model of an undamaged specimen containing a single hole, in order to determine the stress state responsible for initiating tangential splits. The results indicate that the splits are driven by shear stresses parallel to the 0° fibres and small tensile transverse stresses. Further details are given in the Appendix.

The stress distribution in the damaged laminate was also modelled using the finite element method. The laminate is treated as a linear elastic material with the elements in the damaged region, above and below the hole, having reduced stiffness properties in an attempt to represent the effect of the damage. A far-field uniform stress, σ^{∞}, is applied to the

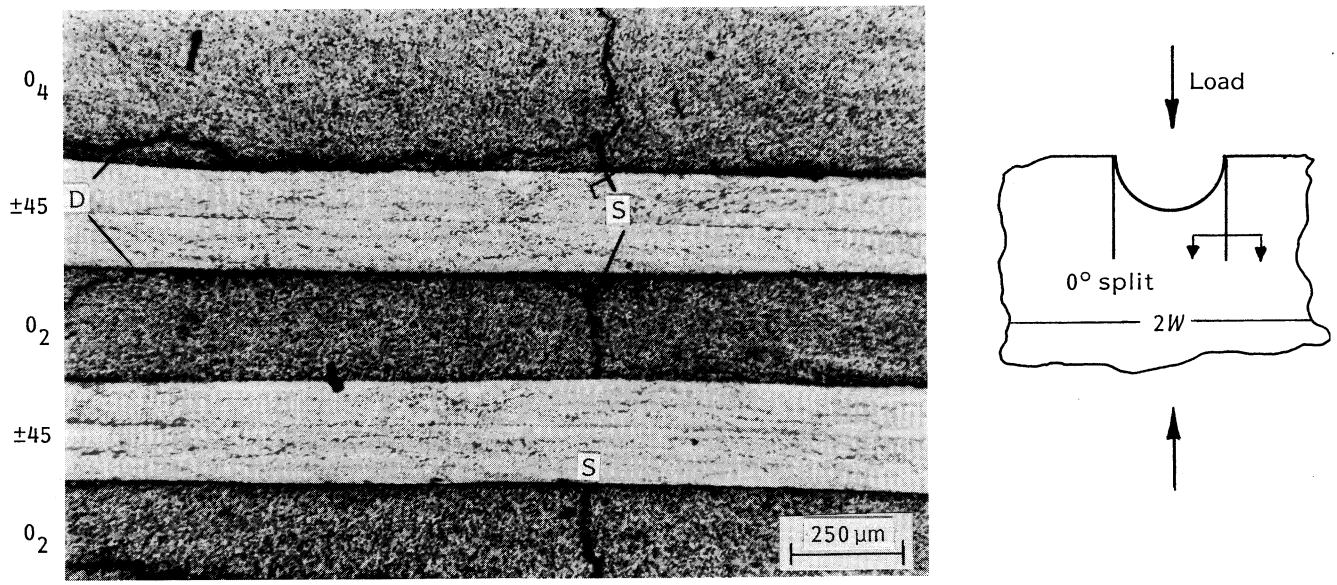

Fig. 4 Transverse section of compression–compression fatigue damaged laminate. σ_{max} = 75% σ_{ult}, N = 10^6, ply thickness = 0.125 mm. The arrows marked 'D' denote delamination, while the arrows marked 'S' denote splitting

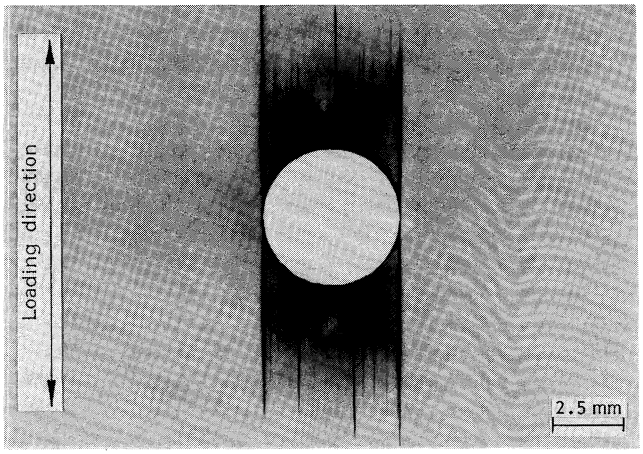

Fig. 5 Compression–compression damage in a specimen cycled continuously up to 10^6 cycles at σ_{max} = 85% σ_{ult} (=365 MPa)

model. The finite element mesh is constructed using second-order (eight-node) plane stress isoparametric elements. Figure 6(a), shows the elements around the hole region in the finite element mesh used in the present analysis. The damage zone consists of splits tangent to the hole, marked as region A in Fig. 6(a), and delamination above and below the hole, marked as region B in the same figure.

The stiffness properties used for the undamaged material are: E_{yy} = 92 GPa, E_{xx} = 26 GPa, G_{xy} = 23 GPa and ν_{yx} = 0.69 (see Soutis and Fleck[2]). The x–y Cartesian coordinates have an origin at the centre of the hole as shown in Fig. 6(a).

The splits and the delamination are represented by reducing the transverse stiffness, E_{xx}, and Poisson's ratio, ν_{xy}, to zero in the 0° plies, in the shaded regions of the mesh shown in Fig. 6(a). The reduced stiffness properties of these shaded regions, analysed as homogeneous elements, are then found from laminate plate theory, giving

E_{yy} = 92 GPa, E_{xx} = 19.6 GPa,

G_{xy} = 23 GPa and ν_{yx} = 0.74.

The calculated stress distribution, $\sigma_{yy}(x, 0)$, for a model laminate with a single hole and fatigue damage consisting of splits of half-length l_s = 2.4R and delaminated region of half-length l_d = 1.2R (hole radius R=2.5 mm) is shown in Fig. 6(b). The length of the damage zone in the model is equal to the observed split length shown in Fig. 5. The stress distribution of the undamaged orthotropic laminate is also plotted in Fig. 6(b) for comparison. It can be seen that the maximum stress σ_{yy} at the edge of the hole of the 'damaged' laminate has been reduced by nearly 16% when compared to the 'undamaged' laminate. This reduction is of similar magnitude to the increase in residual strength of the fatigue damaged laminate. This is encouraging given the simplicity of the approach.

Further work is required; the problem is three-dimensional and the interlaminar normal stress and shear stresses at the hole edge, which are responsible for the initiation of delamination, need to be considered. The finite element analysis used here was a preliminary one with the aim being to show that the elements with reduced stiffnesses can influence the stress distribution significantly.

Experimental results and discussion, two-hole specimens

Stress–life data

The stress versus life, S–N, data for the $[(\pm 45/0_2)_3]_s$ composite laminate with two holes spaced edge-to-edge by one radius are plotted in Fig. 7. At a maximum cyclic compressive stress of σ_{max} = 90% σ_{ult} (=300 MPa), the laminate fails in fatigue after approximately 10^5 cycles as a result of progressive fibre microbuckling. When the test is interrupted repeatedly and zinc iodide solution is applied failure occurs at the grip after more than 10^5 cycles, see Fig. 7. It seems that zinc iodide solution accelerates split growth and microbuckling is arrested. Specimens tested with or without penetrant at cyclic compressive stresses of σ_{max} = 75% σ_{ult} and 85% σ_{ult} survive more than 10^6 cycles.

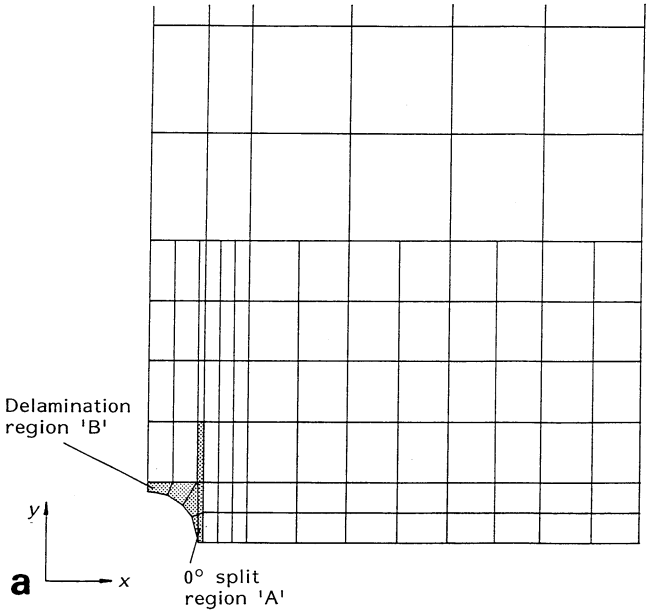

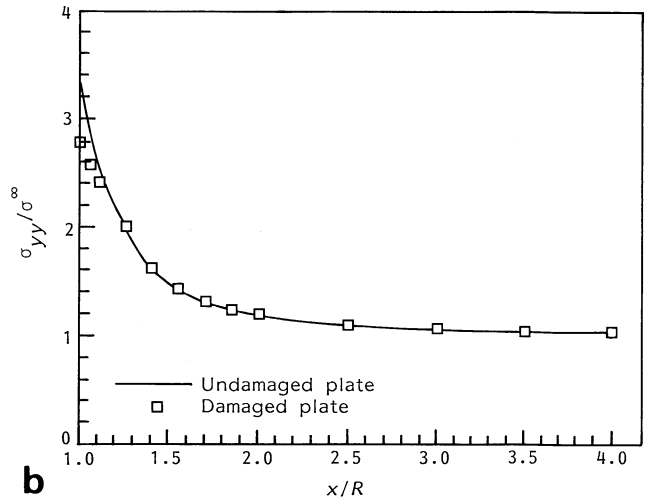

Fig. 6 (a) Finite element mesh used to calculate the stress distribution, $\sigma_{yy}(x, 0)$, in the compression–compression fatigue damaged T800/924C plate. The reduced stiffness elements are shaded. (b) Stress distribution, $\sigma_{yy}(x, 0)$, for damaged and undamaged T800/924C orthotropic laminate

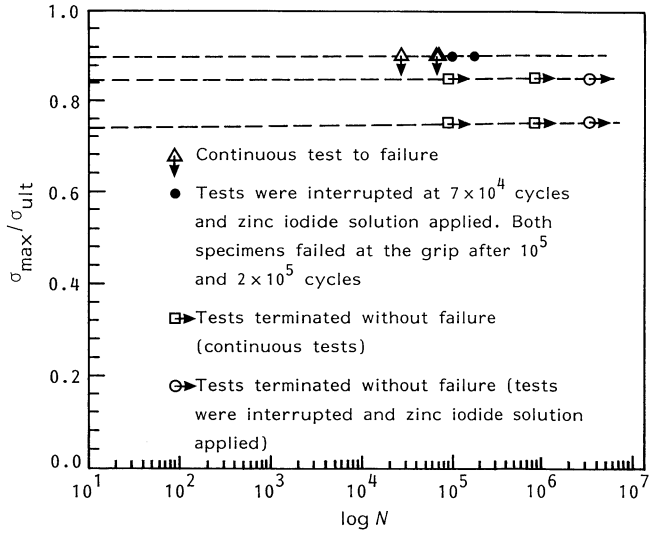

Fig. 7 *S–N* data for specimen with two holes one radius apart (edge–edge). Load ratio, $R = 10$

Damage development in fatigue

$\sigma_{max} = 75\% \sigma_{ult}$

Specimens fatigued at a stress level $\sigma_{max} = 75\% \sigma_{ult}$ (=250 MPa) show splitting tangential to the holes in the 0° layers and subsequent splitting of the off-axis plies, prompting delaminations. Delaminations develop between the 0° and ±45° laminae, in areas which have seen extensive matrix cracking. Fig. 8(a) shows the damage pattern on a specimen cycled continuously for 10^6 cycles. The 45° matrix cracks in the region between the holes occur in the outer angle plies after 10^5 cycles. As cycling of the laminate is continued the extent of matrix cracking and delamination increases. After 4×10^6 cycles the matrix in the area between the notches has deteriorated via intralaminar and interlaminar cracking to the point when fibres have little or no matrix support and fail by buckling under the compressive load, see Fig. 8(b). However, the region outside the holes can accommodate the extra stress and little further damage occurs there. The splits in the 0° layers have isolated the holes from the rest of the laminate in a similar way to the single-hole specimen described earlier. These splits reduce the stress concentration at the outer hole edges sufficiently to prevent microbuckling.

$\sigma_{max} = 85\% \sigma_{ult}$

X-ray photographs of the damage sequence in a specimen fatigued at a stress level of $\sigma_{max} = 85\% \sigma_{ult}$ (=280 MPa) are shown in Fig. 9. In the first cycle, microbuckling failure occurs between the two holes with associated delamination; fibre microbuckles of length 0.4 mm also form at the outside edges of the holes. As shown in Fig. 9(a), a few matrix cracks develop at the top and bottom of the holes (the dark circular area around the holes is drilling damage and is retained within

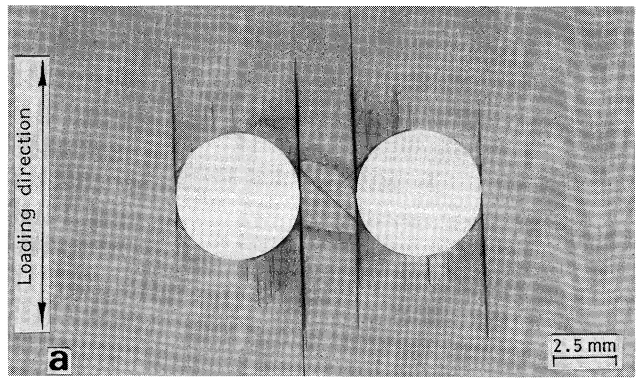

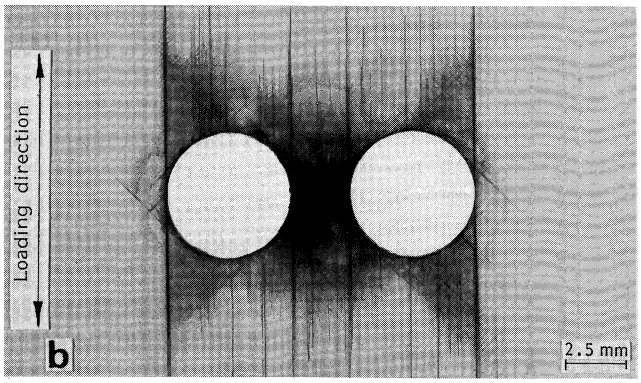

Fig. 8 (a) Damage on a specimen cycled with no interruption up to 10^6 cycles at 75% σ_{ult} (250 MPa). (b) Fatigue damage after 4×10^6 cycles. Hole diameter = 5 mm

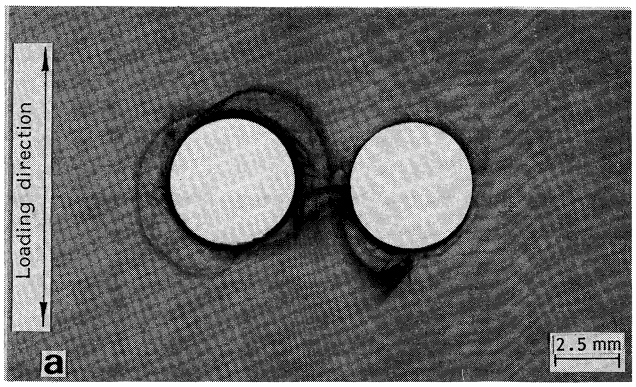

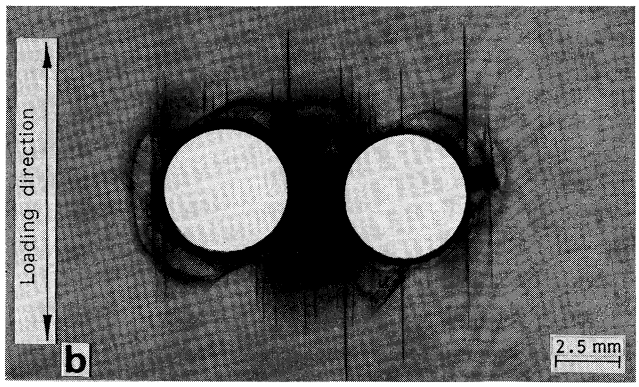

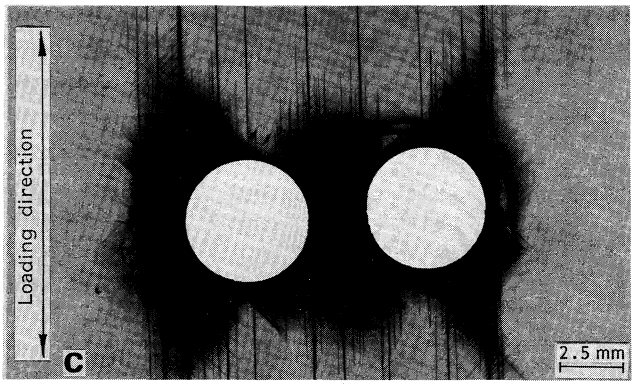

Fig. 9 X-ray radiographs illustrating compression–compression fatigue damage on a specimen with two holes cycled at a stress level of 85% σ_{ult} (=280 MPa). (a) N = 1. (b) N = 10^5 cycles. (c) Damage after $N = 4 \times 10^6$ cycles. Fibre microbuckling has been arrested by the 0° splits. Hole diameter = 5 mm

the surface plies). After 10^4 cycles more splitting has occurred in the 0° and off-axis plies, mainly in the narrow strip between the holes, while the fibre microbuckling at the outside edges of the holes has grown by 0.7 mm. After 10^5 cycles these microbuckles have extended to 1.8 mm, see Fig. 9(b). This buckled region is surrounded by delamination and includes some axial and off-axis ply cracks. At 10^6 cycles the fibre buckling stops growing in the transverse direction of the specimen because matrix cracking arrests and blunts the tip of the microbuckle. The 45° splits have become more numerous and longer. Delamination grows away from the hole, parallel to the load direction, but is arrested in lateral growth by the presence of the splits in the 0° layers. Fig. 9(c) shows the damage after 4×10^6 cycles and it appears to be well contained between axial splits close to the edges of the holes.

The relative growth rates of the microbuckle (emanating transversely from the hole edge) and the vertical splits (propagating tangentially from the hole edges) determine whether fatigue failure will occur by fibre microbuckling. In the absence of splitting, the stress intensity at the tip of the microbuckle increases as its length increases; one expects a corresponding increase in fatigue crack growth rate, leading to laminate fracture. This does not occur due to the presence of splits. Figure 10 displays the growth rate of the split (measured from radiographs) and the microbuckle growth rate as functions of their respective lengths, for the specimen fatigued at σ_{max} = 85% σ_{ult}. As the buckle length increases its growth rate decreases. This is a result of the split (and associated damage) growth lowering the stress concentration in the region of the microbuckle tip. Eventually the microbuckle is arrested.

In order to examine the compression–compression fatigue damage at σ_{max} = 85% σ_{ult} in more detail a transverse section was made through the holes on a specimen fatigued for 10^6 cycles, as shown in Fig. 11(a). The splits in the 0° layers do not propagate into adjacent off-axis plies. They are generally arrested by the ply interface which delaminates. Sometimes the 0° splits grow to the neighbouring ±45° plies by linking a ply crack with delamination or with a resin-rich region in the interface as shown in Fig. 11(a). Longitudinal sectioning shows the fibre microbuckling in the 0° layers, see Fig. 11(b). The dark, voided region is due to damaged material in the buckled zone falling out during the polishing process. Local delaminations are present at the −45°/0° and +45°/0° interfaces

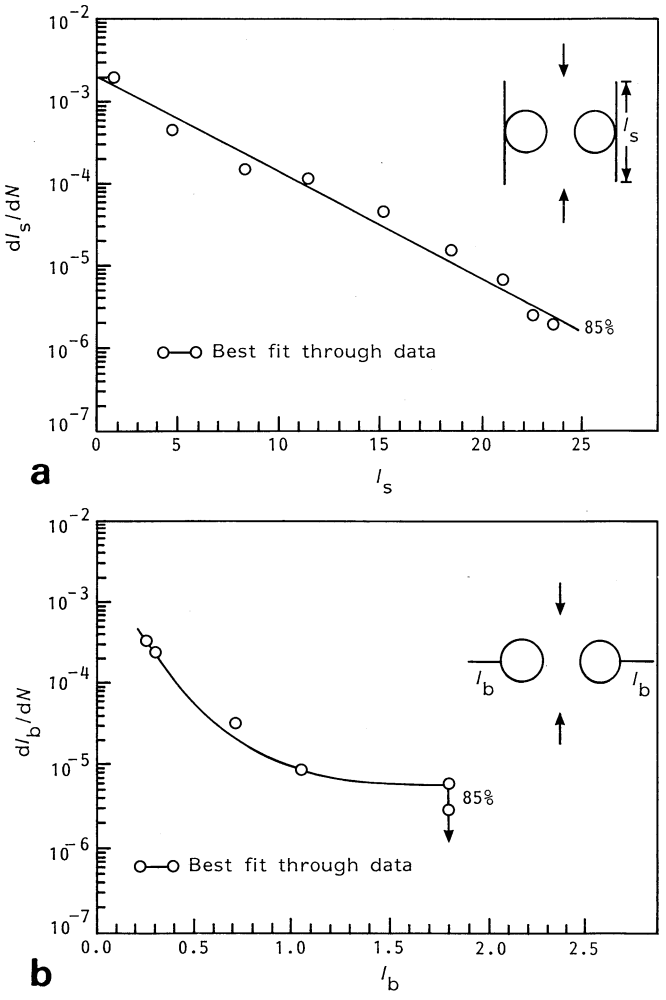

Fig. 10 (a) Split growth rate versus split length for a two-hole specimen (one radius apart) cycled at a stress level of 85% σ_{ult}. (b) Microbuckling growth rate versus buckling length

to accommodate the large fibre rotations and displacements that occur locally. From the X-ray radiography it was observed that these delaminations do not propagate across the width of the laminate. In Fig. 11(b), matrix cracking in the ±45° plies can also be seen.

$\sigma_{max} = 90\%\ \sigma_{ult}$

For specimens fatigued at a stress level of 90% σ_{ult} (=300 MPa) progressive microbuckling from the outer hole edges causes final failure in less than 10^5 cycles. Three specimens were fatigued at this stress level without interruption and they failed after 3×10^4, 7.5×10^4 and 7.8×10^4 cycles. The fibre microbuckling growth rate exceeds the rate of vertical splitting, thus precluding any stress reducing effect that usually attends splitting. An additional specimen was cycled at 90% of the notched strength, and the test was stopped after 7×10^4 cycles for damage examination, see Fig. 12. The damage consists of 0° tangential splits and many small ±45° ply cracks. Material in the region between the holes is heavily damaged by matrix cracking, delaminations and fibre microbuckling. Fibre microbuckling is present at the outside edge of the holes. After the X-ray examination this specimen was cycled to failure; the specimen failed by the splits growing into the grips after 2×10^5 cycles. This is probably due to the presence of the zinc iodide solution which accelerates the split growth. The splits grow faster than the buckled regions and the fibre microbuckling is arrested.

Residual compressive strength measurements

Specimens cycled continuously at a stress level of 75% σ_{ult} (=250 MPa) for 10^5, 10^6 and 4×10^6 cycles had residual compressive strengths of 331, 365 and 392 MPa, respectively, compared with a static notched strength, σ_{ult}, of 330 MPa, see Fig. 13. These specimens were not treated with zinc iodide solution. The increase in residual strength is related to the progressive removal of the stress concentration effect of the

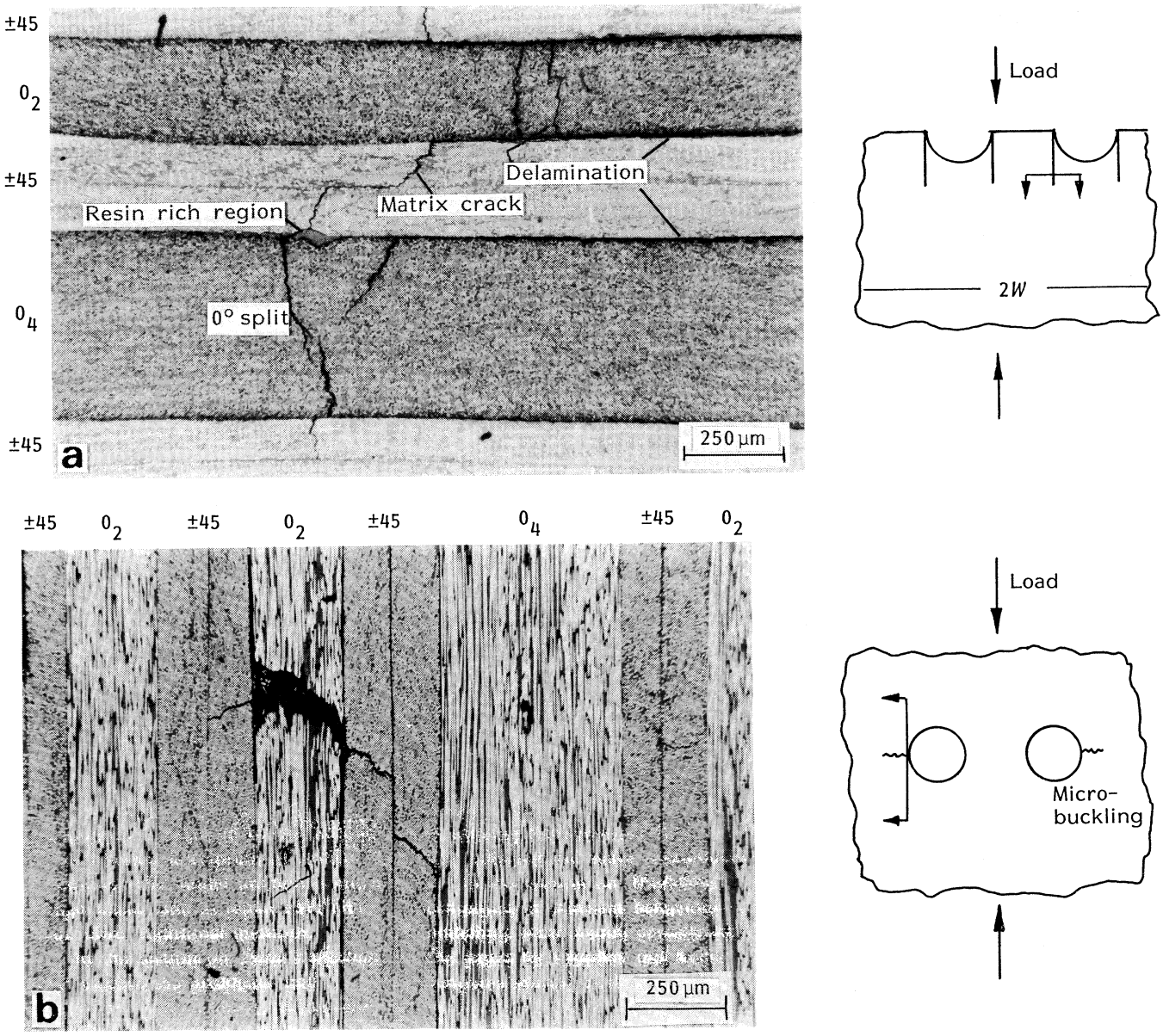

Fig. 11 (a) Transverse cut on a specimen with two holes, one radius apart, cycled at 85% σ_{ult} (=280 MPa) for 10^6 cycles. (b) Longitudinal section revealing fibre buckling in the 0° layers. Local delaminations are present at the +45/0 and −45/0 interfaces and also some off-axis ply cracks. The specimen is again with two holes, one radius apart, cycled in compression at 85% σ_{ult} to 10^6 cycles. Ply thickness = 0.125 mm

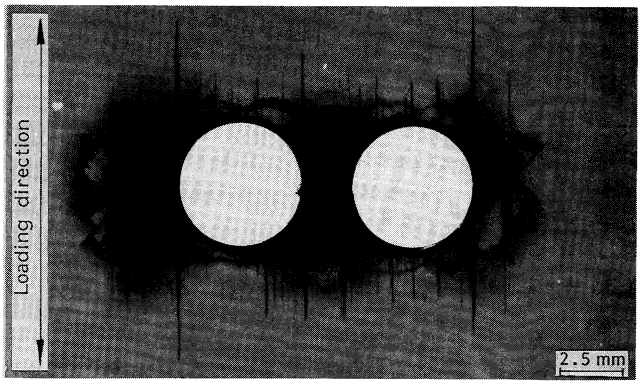

Fig. 12 Compression–compression fatigue damage on a specimen cycled at 90% σ_{ult} up to 7×10^4 cycles

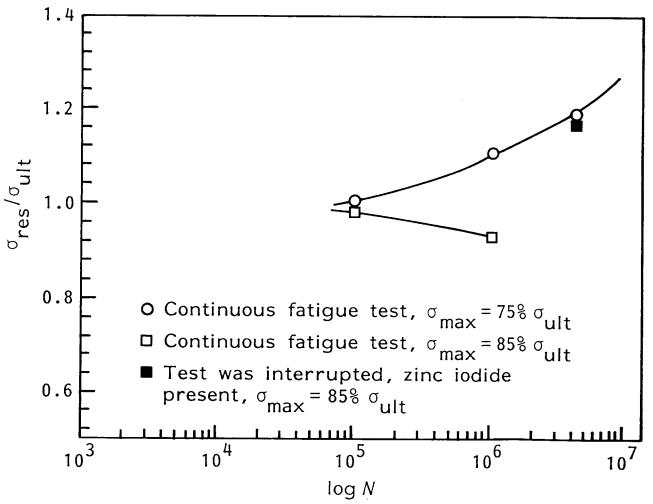

Fig. 13 Residual strength normalized by the static failure stress versus the number of cycles for a two-hole specimen

holes through splitting and delamination, as discussed for the single-hole specimens. Interestingly, the damage responsible for the stress redistribution (*ie* splitting and delamination) is not part of the fracture surface. Splitting and delamination grew axially above and below the hole, but the fracture is transverse. Thus, unlike in metals, the initiation of damage at a hole leads to a reduction of the stress concentration and may, in part, explain the damage tolerance of these fibrous systems.

Specimens cycled continuously at a higher stress level, 85% σ_{ult} (=280 MPa) for 10^5 and 10^6 cycles have compressive residual strengths of 325 and 307 MPa, respectively. These specimens were not treated with penetrant. The marginally greater strength degradation from the longer fatigue cycling is probably associated with the fact that the buckled zones have propagated further across the laminate's width. The specimen of Fig. 9(c) received zinc iodide treatment and was cycled at the same high stress level (σ_{max} = 85% σ_{ult}) for 4×10^6 cycles. Its compressive residual strength was 384 MPa, which is 15% higher than the notched static strength σ_{ult}. This increase in strength is due to accelerated split growth associated with the zinc iodide solution. Fibre microbuckling was arrested during fatigue loading of the specimen.

Concluding remarks

Compression–compression fatigue damage in notched $[(\pm45/0_2)_3]_s$ composite laminates consists of matrix cracking, delaminations and, at applied compressive stresses approaching the laminate strength, fibre microbuckling.

In single-hole specimens at a stress level, σ_{max}, equal to 75% of the static notched compressive strength σ_{ult}, damage in the form of intra- and interlaminar cracking extends along the longitudinal axis of the laminate parallel to the applied load and is well contained between axial splits at the edges of the hole. This type of damage lowers the stress concentration around the hole. Fatigue cycling at this load level results in residual strengths greater than the notched static strength. A two-dimensional finite element analysis of a model possessing characteristic 'damage' revealed that the stress concentration factor in the 'damaged' model is reduced by 16% compared to that in an 'undamaged' model. This agrees with the magnitude of residual strength increase measured in the 'damaged' laminates. The longitudinal stiffness of the specimen undergoes a small reduction in value during cycling loading; this is associated with the fact that the damage is restricted to the vicinity of the hole. When σ_{max} in the fatigue cycle equals 90% σ_{ult}, fibre microbuckling extends in the transverse direction and causes fracture of the laminate in less than 10^5 cycles.

Similar behaviour is observed in the two-hole specimens. In these specimens it is possible to obtain a quantitative estimate of the microbuckle growth rate as well as the split growth rate. For σ_{max} = 85%σ_{ult}, microbuckles initiate and grow, but are arrested subsequently by growth of the 0° longitudinal splits tangential to the outer edges of the holes. The splits serve to reduce the stress concentration in the vicinity of the holes.

A penetrant consisting of a zinc iodide solution affects damage development in the notched composite laminates. It increases the split growth rate, which reduces the stress concentration due to holes and tends to arrest fibre microbuckling. Thus the application of penetrant prolongs the fatigue life of the specimens tested in this investigation.

Acknowledgements

The authors are grateful for funding from the Procurement Executive of the Ministry of Defence, under a joint SERC/MOD contract. We would like to thank Dr P.T. Curtis of the Royal Aerospace Establishment, Farnborough for many helpful discussions.

Appendix

Stress analysis of undamaged specimen

The in-plane stresses in an undamaged specimen containing a single hole were calculated using an elastic version of the MARC finite element program.[9] The laminate is modelled as a two-dimensional linear elastic orthotropic material, using eight-node plane stress isoparametric elements. The laminate stiffness properties are derived from unidirectional properties via laminate theory; they are: E_{yy} = 92 GPa, E_{xx} = 26 GPa, G_{xy} = 23 GPa and ν_{yx} = 0.69, where x is the transverse direction and y is the loading direction.

Laminate theory is also used to extract the ply stresses from the results for the homogeneous body. Contours of constant stress components σ_{yy}, σ_{xx} and σ_{xy} are presented in Fig. A1 for the 0° layers in the vicinity of the hole. As expected, there is a large stress concentration at the edge of the hole such that the stress σ_{yy} (parallel to the 0° fibres) exceeds 5.5 times the remote average stress σ^∞ on the specimen. Splitting of the 0° plies develops tangentially to the hole, along the path shown in Fig. A1. We assume an in-plane

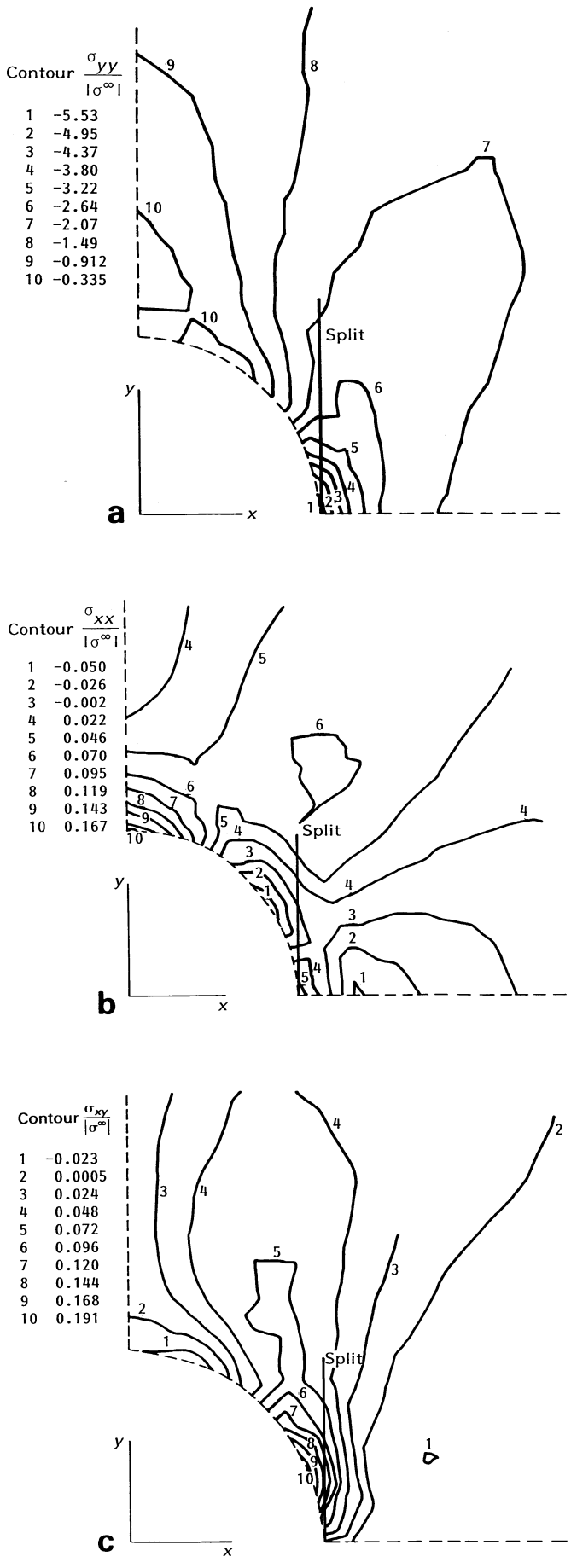

Fig. A1 In-plane stress contours in the 0° layer of the T800/924C orthotropic plate ($\sigma^{\infty}=1.0$). (a) σ_{yy} parallel to the fibres. (b) σ_{xx} perpendicular to the fibres. (c) σ_{xy} shear stress contours

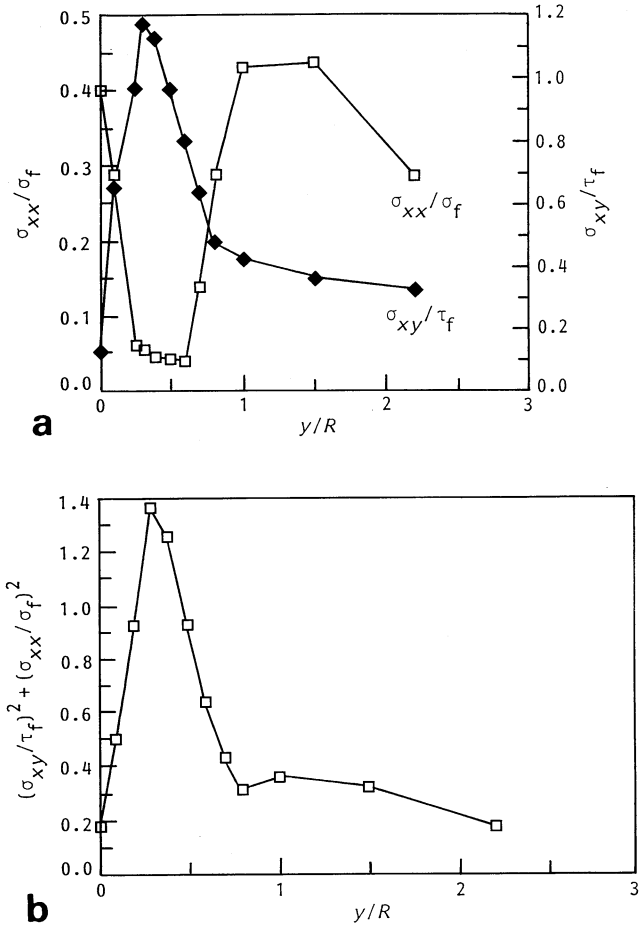

Fig. A2 (a) Local stresses σ_{xx} and σ_{xy} in the 0° ply normalized by the transverse failure strength and shear strength, respectively, along the line $x=R$ ($\sigma^{\infty}=0.9\ \sigma_{ult}$). (b) Tsai–Hill fracture criterion to predict splitting in the 0° ply at $x=R$ ($\sigma^{\infty}=0.9\ \sigma_{ult}$)

shear strength τ_f of 105 MPa and a transverse tensile strength σ_f of 63 MPa for the 0° plies. Along the line of splitting the ratio of shear stress σ_{xy} to shear strength τ_f is much higher than the ratio of transverse stress σ_{xx} to transverse strength σ_f, as shown in Fig. A2(a).

The severity of the stress state along the line of splitting can be gauged by assuming that splitting occurs when the Tsai–Hill failure criterion is satisfied,

$$f(\sigma) \equiv \left(\frac{\sigma_{xy}}{\tau_f}\right)^2 + \left(\frac{\sigma_{xx}}{\sigma_f}\right)^2 = 1 \qquad \text{(A1)}$$

Here, it is assumed that splitting occurs under static loading when $f(\sigma) = 1$. In static tests it has been found that splitting initiates when σ^{∞} equals 90% of the static notched compressive strength σ_{ult} of the laminate. A plot of $f(\sigma)$ along the line of splitting is given in Fig. A2(b), for this load level. We find that $f(\sigma)$ exceeds unity for $0.2 \leq y/R \leq 0.5$; the Tsai–Hill criterion is in fair agreement with the observation of initiation of splitting in the static tests when $\sigma^{\infty} = 90\%\ \sigma_{ult}$. Further, we conclude from Fig. A2(a) that the shear stresses drive the splitting.

Splitting occurs at lower load levels in fatigue than under static loading. For example, extensive splitting occurs when the maximum load of the fatigue cycle equals 75% of σ_{ult}, as shown in Figs 1(b) and (c).

References

1. **Soutis, C.** 'Compressive failure of notched carbon fibre–epoxy panels' *PhD Thesis* (Cambridge University Engineering Department, UK, 1989)
2. **Soutis, C. and Fleck, N.A.** 'Static compression failure of carbon fibre T800/924C composite plate with single hole' *J Comp Mater* to be published
3. **Purslow, D. and Potter, R.T.** 'The effect of environment on the compression strength of notched CFRP—a fractographic investigation' *Composites* **15** 2 (1984) pp 112–129
4. **Guynn, E.G. and Bradley, W.L.** 'A detailed investigation of the micromechanics of compression failure in open hole composite laminates' *J Comp Mater* **23** (1989) pp 479–504
5. **Soutis, C., Fleck, N.A. and Smith, P.A.** 'Strength prediction technique of notched CFRP laminates with circular holes' Submitted to *J Comp Mater* (February 1990)
6. **Curtis, P.T.** 'Investigation of the mechanical properties of important carbon fibre reinforced materials' *RAE TR-86021* (1986)
7. **Whitcomb, J.D.** 'Experimental and analytical study of fatigue damage in notched graphite/epoxy laminates' *Fatigue of Fibrous Composite Materials, ASTM STP 723* (1981) pp 48–53
8. **Black, N.F. and Stinchcomb, W.W.** 'Compression fatigue damage in thick notched carbon–epoxy laminates' *Long Term Behavior of Composites, ASTM STP 813* (1983) pp 95–115
9. **MARC Finite Element Package** (MARC Analysis Research Corporation, Palo Alto, California, USA)

Authors

C. Soutis and N.A. Fleck are at Cambridge University Engineering Department, Trumpington Street, Cambridge CB2 1PZ, UK. P.A. Smith is in the Department of Materials Science and Engineering, University of Surrey, Guildford, Surrey GU2 5XH, UK.